

 **DOR: 20.1001.1.2322388.2021.9.1.1.7**

Research Paper

Dissimilar DP780/DP980 Resistance Spot Welded joints: Microstructure, Mechanical Properties and Critical Diameter

Bahman Valizadeh, Mehdi Mansouri**Advanced Materials Research Center, Department of Materials Engineering, Najafabad Branch, Islamic Azad University, Najafabad, Iran*

ARTICLE INFO*Article history:*

Received 19 May 2020
Accepted 2 July 2020
Available online 3 January 2021

Keywords:

*Dissimilar Resistance Spot
Welding
DP780 Dual Phase steel
DP980 Dual Phase steel
critical weld nugget diameter
mechanical behavior*

ABSTRACT

In this research, microstructure and mechanical performance of dissimilar resistance spot welded DP780/DP980 dual-phase steels were studied utilizing optical microscope, microhardness, and tensile shear tests. Resistance spot welding (RSW) was performed in the current range of 7 to 12 kA, with 0.5 kA steps. At welding currents lower than 7 kA low amount of melting led to the very low strength of the joints due to small weld nugget diameter. The results showed that an increase in welding current from 7 kA up to 11 kA, result in an increase in weld nugget diameter. Further increase of welding current (higher than 11 kA), however decreased the weld nugget diameter due to severe melt expulsion. Microstructural studies showed that weld nugget was primarily comprised of martensite, and the heat-affected zone (HAZ) of both sides of the joint was comprised of three different microstructural zones; upper-critical HAZ (UCHAZ), inter-critical HAZ (ICHAZ), and sub-critical HAZ(SCHAZ). Microhardness test showed that at both sides, softening occurred at SCHAZ. The results of the tensile shear test showed that both peak load and fracture energy of the joints followed approximately the same trend as weld diameter with welding current. Two different fracture modes of interfacial failure (IF) and pullout failure (PF) were observed in the tensile-shear test. At welding currents lower than 10 kA, the failure occurred in IF mode, while at higher welding currents, PF was dominant. Weld nugget diameter at welding current of 10 kA; i.e., critical weld nugget diameter, was ~8.5 mm.

* Corresponding Author:

Email Address: MMansouri@pmt.iaun.ac.ir

1. Introduction

The resistance spot welding is one of the most important joining processes in sheet metal joining, particularly in the automotive industry, due to its high operation speed and suitability for automation. In the RSW process, heat is generated due to localized flow of electrical current through the parts being welded, according to Joule's law ($Q=RI^2t$, Where Q is generated heat, R is electrical resistance, and I and t are welding current and time, respectively). This heat causes to rise in the temperature at the interface of the workpieces that results in the melting of the workpieces and finally forming the weld nugget between the workpieces after solidification. It is worth noting that typically there are about 2000-5000 spot welds in a modern vehicle and the vehicle crashworthiness strongly depends on the mechanical performance of these spot welds [1]. On the other hand, weight reduction in the automotive industry, due to its role in the reduction of fuel consumption, has always been of great importance for manufacturers [1,2]. However, reduction of weight without safety considerations is not desirable, and then increase of the vehicle strength/weight ratio has attracted much attention of researchers and car manufacturers [3]. To increase the strength to weight ratio, utilization of low-density materials such as high strength aluminum alloys or using high strength alloy such as Advanced High Strength Steels (AHSS) for different parts of vehicles is very prevalent [4,5]. Among AHSSs, Dual Phase (DP) steels are one of the most utilized AHSSs in the automotive industry. DP steels, due to their special dual-phase microstructure (hard martensitic islands in a ductile ferrite matrix), exhibited both high strength and ductility. These steels that have almost similar physical properties are named by their ultimate tensile strength, e.g., DP780 has an ultimate tensile strength of ~780 MPa [6–8].

But it must be noted that the challenges of DP steel application in the automotive industry depend on their metallurgical interactions with other body parts in similar and dissimilar welding processes. Severe changes in hardness at weld zone and heat-affected zones [1,9] and higher susceptibility to shrinkage voids during solidification [3,10] are the most important challenges in similar and dissimilar welding of DP steels. Additionally, the complex microstructural changes occurring during welding of DP steels make it hard to determine failure mode and implement the standard to predict important quality control parameters such as critical welding diameter. Therefore, adjustment of RSW parameters in order to achieve desirable mechanical properties for spot welds has drawn the attention of many researchers [11]. Considering the substantial role of resistance spot welds in crashworthiness, studying the mechanical and microstructural properties of the spot welds in order to guarantee the occurrence of pullout failure during loading is crucial [2,12]. Therefore, in this research, the microstructural and mechanical properties of dissimilar DP780/DP980 resistance spot welds were investigated. Samples have been welded at different welding currents, then microstructural and mechanical investigations (in terms of peak load and fracture energy in tensile-shear test) have been carried out.

2. Experimental procedure

DP780 and DP980 steel sheets manufactured by inter-critical annealing process (heating the steel up to the two-phase ferrite+austenite region and then quenching of steel in order to promote the transformation of the formed austenite into martensite) were used as starting materials. The thickness of both DP780 and DP980 sheets was 2 mm. Table 1 shows the chemical composition of the DP780 and DP980 steel base metals.

Table.1 The chemical composition of started materials in present study (wt.%).

	%C	%Mn	%Si	%S	%P	%Ni	%Cr	%Fe
DP780	0.11	2.15	0.08	<0.01	<0.01	0.05	0.15	Bal.
DP980	0.14	2.45	0.05	<0.01	<0.01	0.04	0.25	Bal.

Welding specimens were cut to the size of 138 mm × 60 mm according to AWS D8.9 standard (Fig. 1). Oxides and contaminations on the faying surface of samples were removed, and then samples were set in joint lap configuration with an overlap of 45 mm. One spot weld was made at the center of the overlapped area for each joint. The welding process was carried out using a 120 kVA AC RSW machine (CU900, Novin Sazan co., Tehran, Iran) using a 45° truncated cone copper-chromium-zirconium

electrode (group A class II of RWMA classification) with 8 mm face diameter. The welding current was set from 7 to 12 kA with 0.5 kA steps. Other resistance welding parameters including pre-squeezing time (the period of applying a compressive force on the sheets before current passage in order to stabilize pressure and ensure good contact), electrode force (compressive force exerted on the sheets before, during, and after welding), welding time (current passage time) and

holding time (the period of maintaining compressive force after current passage to help better cooling and keeping the integrity of the joint) was set to 15 cycles, 4 kN, 30 cycles and 15 cycles, respectively (each cycle is ~0.02 s).

For each welding current, four samples were welded, three of which were used for tensile-shear test and one used for metallographical studies and microhardness examination. Metallographic samples were prepared using standard metallographic procedures, including grinding, polishing, and etching. Etching was done using 2% Nital solution for the general microstructure and Klemm's I etchant (50 ml water-saturated with $\text{Na}_2\text{S}_2\text{O}_3$ and 1 g $\text{K}_2\text{S}_2\text{O}_5$) to detect retained austenite. Then, the microstructure was examined utilizing the optical microscope (BX51, Olympus, Japan). The volume percentage of ferrite and martensite phases in the microstructure of the base materials was calculated

using ImageJ software. In order to investigate changes in the hardness profile of the welded samples, a microhardness test (Leco PIX2, Struers GMBH, Belgium) was carried out across two lines parallel to the weld interface in several points which were spaced 0.5 mm apart from each other on average. The indentation load and holding time were 100 g and 15 s, respectively. The tensile-shear test was conducted according to AWS D8.9 standard in order to determine the peak load (maximum force endured by the welded sample) and fracture energy (area under the force-displacement diagram up to peak load). The test was carried out by a tension-compression machine (E4486, Instron Inc., USA) with a tension rate of 10 mm/min. The failure mode of the samples after fracture in the tensile-shear test was determined by visual inspection as illustrated in AWS D8.9 standard. Fig. 1 shows the tensile-shear sample schematically.

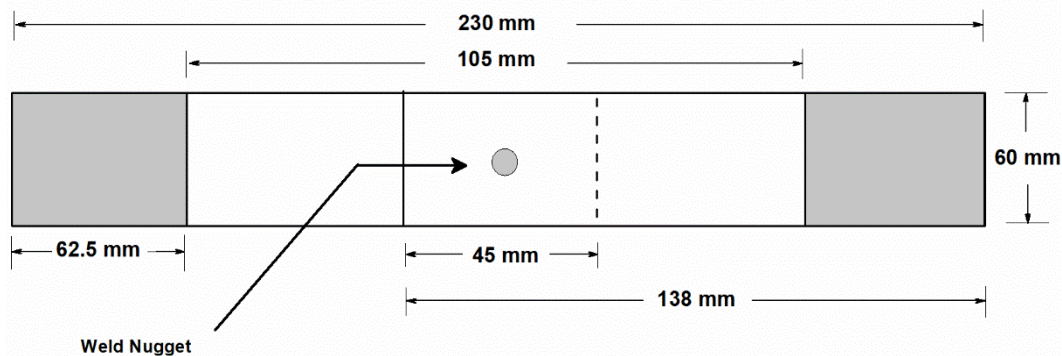


Fig.1. Schematics of a standard tensile-shear test sample.

Peak load is directly extracted from the force-displacement diagram, and fracture energy was calculated using numeral integration (Eq. 1), where F and X are force and displacement, respectively.

$$\text{Fracture energy} = \sum_{n=1}^{n=N} F(n)[X(n) - X(n-1)] \quad (1)$$

Failure modes of welded samples were determined by examining the fractured specimens after the tensile-shear test.

3. Results and discussion

3.1. Macro/microstructure of the weld joints

Fig.2 shows the macrostructure of DP780/DP980 RSW joint welded at 10 kA.

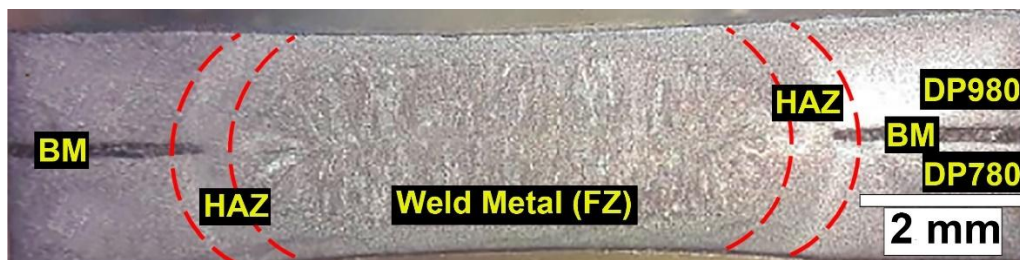


Fig. 2. Macrostructure of DP780/DP980 RSW joint welded at 10 kA.

As demonstrated by Fig. 2, RSW joints exhibit an inhomogeneous microstructure containing weld metal (Fusion Zone, FZ), HAZ (Heat Affected

Zone), and Base Metal (BM). FZ consists of columnar grains, which have grown from the fusion boundary toward the weld centerline and is a result

of the fusion and solidification process. Adjacent to FZ is the HAZ, where no fusion and solidification occur during welding, but as a result of high

temperature, microstructural changes widely occur [1, 10, 13]. Fig.3 shows the microstructure of different zone of the welded sample at 10 Ka.

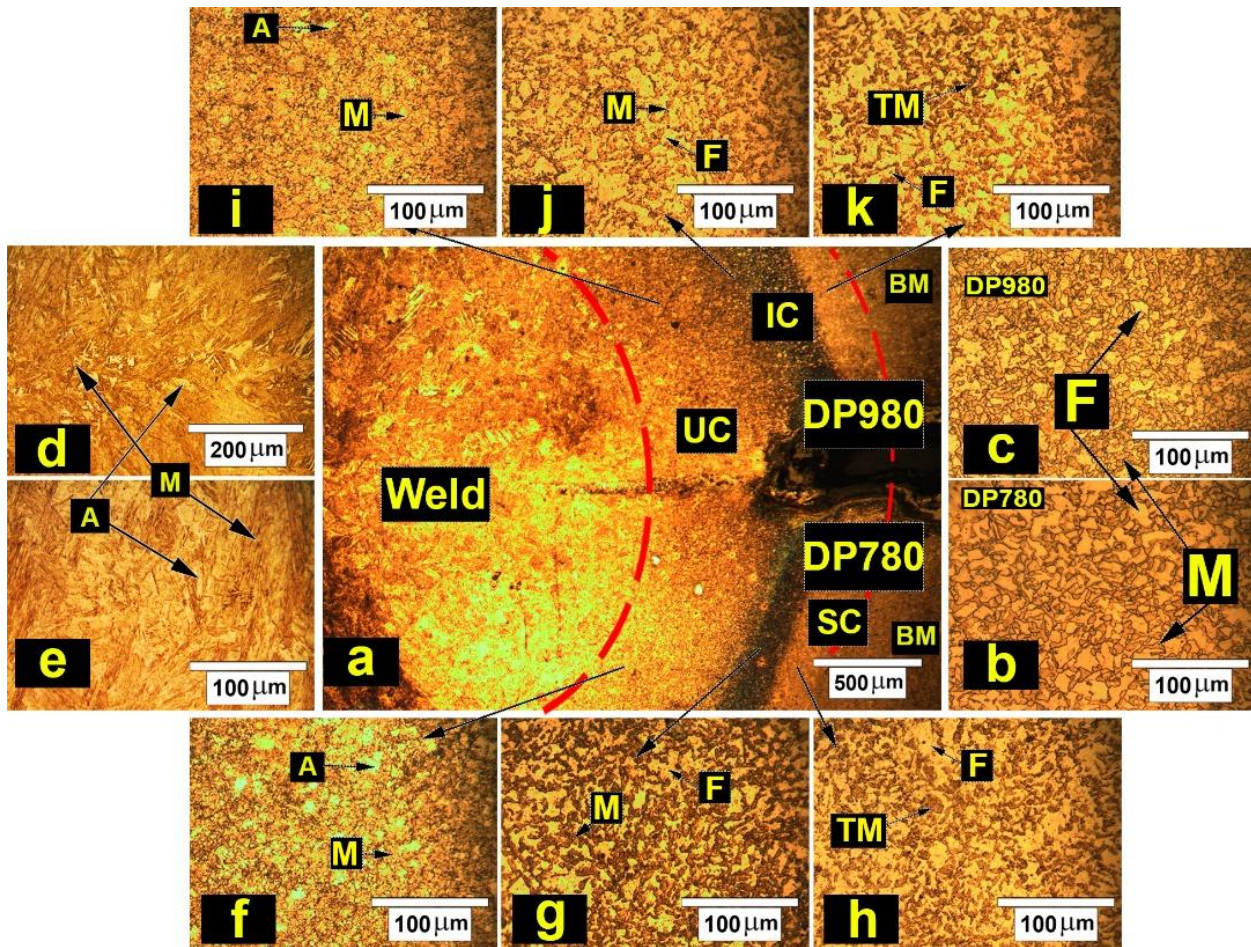


Fig. 3. Microstructure of a) DP780/DP980 resistance spot welded sample at 10 kA, b and c) base materials d and e) FZ, f, g and h) and i, j and k) different regions of HAZ (including upper critical (UC), inter critical (IC) and subcritical (SC)) in DP780 and DP980 sides respectively. A represents retained austenite, F represents ferrite, M represents martensite and TM represents tempered martensite.

Fig.3-b and c show the microstructure of DP780 and DP980 base metals, respectively. In both steels, the microstructure is comprised of martensitic islands in a ferrite matrix. The volume percent of the martensite phase was calculated to be 36% and 43% for DP780 and DP980, respectively.

The microstructure of FZ is presented in Fig.3-d and e. As shown, the FZ microstructure mainly consists of martensite as a result of a very high cooling rate in the RSW process, which is higher than the critical cooling rate for martensite formation. The critical cooling rate at which martensite forms in steels can be calculated from Eq. 2 [10]:

$$\text{Log}V = 7.42 - 3.13C - 0.71Mn - 0.37Ni - 0.34Cr - 0.45Mo \quad (\text{Eq. 2})$$

In this equation, V is the critical cooling rate (in K/h). Assuming that both base metals melt equally to form the weld nugget and using their chemical composition given in table 1, the critical cooling rate for the weld nugget would be ~ 52 °C/s. On the other hand, the analytical results have shown that the cooling rate of a 2 mm thick resistance spot-welded steel sheet is about 3000 °C/s [5]. Then it can be concluded that because of the higher cooling rate of the RSW process (3000 °C/s) that is significantly higher than the critical cooling rate for the weld nugget (~ 52 °C/s) formation of martensite in the FZ is very probable, as shown in Fig.3-d and e. The martensitic structure was also observed at similar and dissimilar joints RSWs of DP steels by other researchers [14–16].

Fig.3-f to fig.3-k show microstructure of different HAZ regions at both DP780 and DP980 sides. Considering microstructural changes, HAZ can be divided into three distinct regions, namely upper critical (UC), inter critical (IC), and subcritical (SC) HAZ [11, 17, 18]. At UCHAZ, the experienced peak temperature by this zone is above the A3 line. Thus the microstructure becomes fully austenitic, and as a result of high temperature near the fusion line, grain growth occurs severely in this region. Austenite grain growth leads to higher hardenability, and austenite transforms into martensite during the cooling cycle. At the ICHAZ region, the peak temperature is lower due to the higher distance from the fusion line, and temperature would not rise above A3 but remains between A3 and A1 (austenite+ferrite region). Therefore, the microstructure would consist of austenite and ferrite, that during cooling, austenite transforms into martensite [1, 18]. At the SCHAZ region, peak temperature would not get higher than the A1 line, so only the tempering of martensite in

the microstructure of the base metals (DP980 and DP780) occurred [19].

3.2. Mechanical properties

3.2.1. Microhardness profile

Fig. 4 shows changes in microhardness profile for the sample welded at 10 kA. As Fig. 4 shows, the average hardness value of FZ is ~410 HV. The high value of hardness at FZ is a result of martensite formation in this region [1, 18]. At the ICHAZ region, both martensite and ferrite are present in the microstructure (Fig.3), and the mean hardness value is lower than FZ (~350-300 HV), but still higher than both DP steel base materials (260 HV and 280 HV for DP780 and DP980 respectively). However, values of hardness at SCHAZ is lower than both base materials (~245 HV). This phenomenon is called HAZ softening and is resulted by tempering of the martensite [19, 20]. Moreover, the amount of softening at the DP980 side is slightly higher, which can be a result of higher martensite content in DP980 base metal.

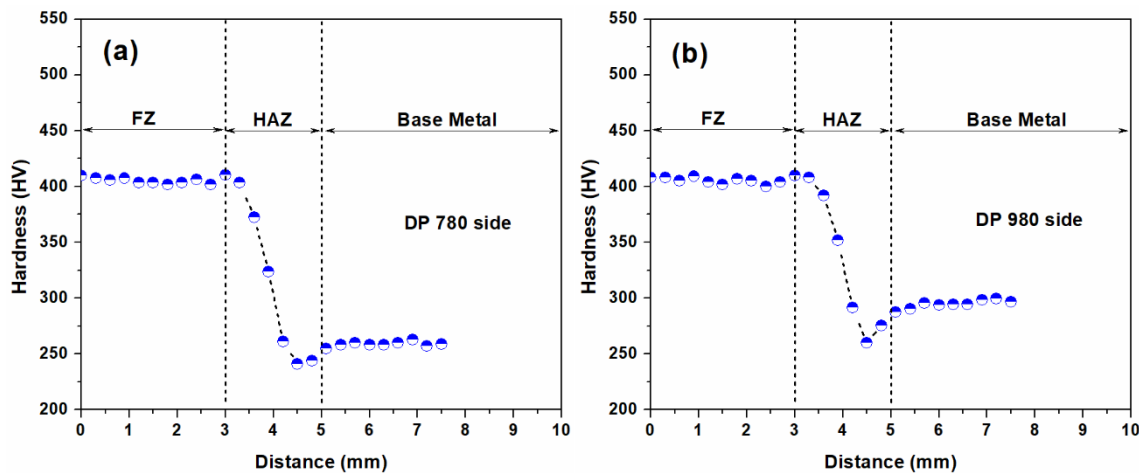


Fig.4. Microhardness profile of different regions of specimen welded at 10 kA, a) DP780 side and b) DP980 side.

3.2.2. Tensile properties and Failure mode

Fig. 5-a shows changes of weld nugget diameter with welding current. Up to 11 kA, weld nugget diameter increases with welding current. The main reason for

the increase is higher heat input and a higher amount of melting, which occurs at the weld interface. Nevertheless, at welding currents higher than 11 kA, the weld nugget diameter decreases as a result of expulsion.

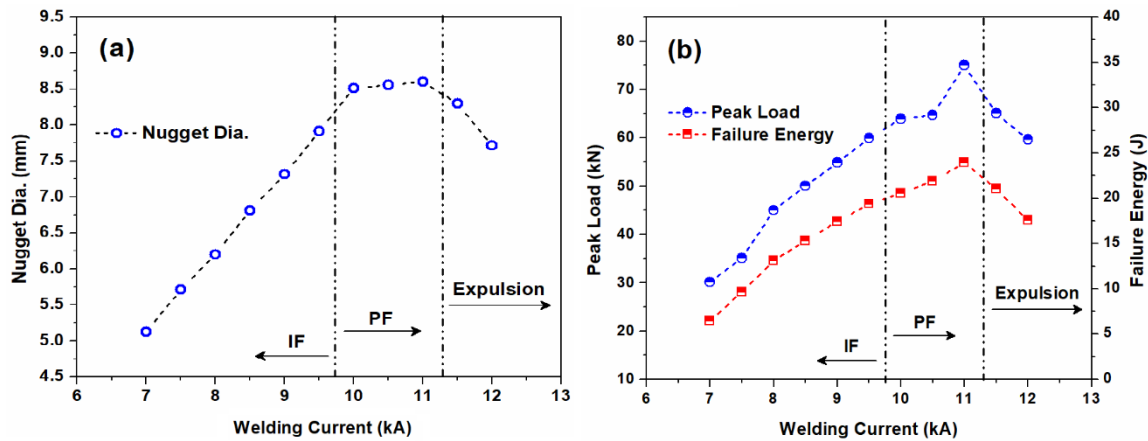


Fig.5. Effect of welding current on (a) Weld nugget diameter and (b) Peak load and failure energy of DP780/DP980 RSWs.

Failure mode was determined by examination of fractured tensile-shear test samples. In Interfacial Fracture (IF) failure mode, the crack propagates through the weld nugget because of the lower strength of weld metal, and the fracture occurs abruptly. On the other hand, at Pullout Fracture (PF) failure mode, failure occurs via withdrawal of the weld nugget from one sheet [1]. Results showed that up to 9.5 kA, the IF mode is the dominant failure mode. By increase in the welding current further than 9.5 kA the failure mode will change to PF mode. The changing of fracture mode is related to the weld nugget diameter. The weld nugget is the load-bearing part of the joint in the tensile-shear test, and the larger the weld nugget becomes, the higher would be the capacity of the joint to endure exerted loads. In weld nugget lower than the critical size, the load-bearing capacity of the weld nugget is lower than its surrounding (i.e., HAZ or BM) due to the small size of the weld nugget then the fracture propagates through the fusion zone (IF mode). By increase in the weld nugget due to an increase in welding current, the load-bearing capacity of the weld nugget increases and becomes more than the load-bearing capacity of the surrounding areas of the weld nuggets. Consequently, the failure occurs via withdrawal of the weld nugget from one sheet, and fracture mode changes from interfacial failure to pullout failure [1]. As shown elsewhere, PF fracture mode exhibits higher peak load and fracture energy than IF mode. Therefore, achieving PF fracture mode is a priority in most spot welding processes [10]. Fig. 5-b shows changes in peak load and fracture energy of the joints welded at different welding currents in the tensile-shear test. Both peak load and fracture energy increase with welding currents up to 11 kA and decrease afterward. The reason for the enhancement of tensile properties can be attributed to an increment of weld nugget diameter, which

increases load-bearing and energy absorption capacity of the joints before expulsion [21, 22].

PF fracture mode in the tensile-shear test usually begins with crack growth around the weld nugget. The difference of mechanical properties between weld nugget and surrounding regions is the main reason for changes in the crack growth path. In fact, the higher load-bearing capacity of the weld nugget leads to alteration of crack growth path from weld nugget (IF mode) to the HAZ (PF mode). Therefore, a critical weld nugget diameter (D_c) is defined as the diameter at which failure mode changes from IF to PF [10, 16].

Multiple theoretical equations have been developed in order to determine D_c [23–26]. For instance, according to the JIS Z3144 standard [25], the minimum weld nugget diameter in order to achieve PF mode can be calculated from Eq. 3.

$$D_c = 5\sqrt{t} \quad (3)$$

In which t is the thickness of base sheets. Utilizing eq.3, the critical nugget diameter calculated for the sheets used in this study becomes ~ 7.1 mm. The actual critical nugget diameter for failure mode transition in this research was ~ 8.5 mm, however, which is far larger than JIS Z3144 standards prediction and certifies that the standard equations cannot predict D_c for the DP780/DP980 RSW joints correctly. The main reason for this is the complexity of microstructure and mechanical properties of dissimilar joints made of DP steels. Thus, the equations which only use geometrical parameters to predict the critical FZ size could not correctly predict D_c for DP steels [23]. In order to address this issue, Pouranvari et al. [28] have developed a model which, in addition to plate thickness, takes into account the mechanical properties of the joints made of AHSS steels. In this model, D_c in the tensile-shear test is calculated using Eq. 4:

$$D_c = \frac{4t}{P_f} \cdot \frac{H_{PFL}}{H_{FZ}} \quad (4)$$

where t is the thickness of the base sheets, P is the porosity factor, f is the tensile strength/shear strength ratio, and $HPFL$, HFZ is the hardness of pullout failure location and FZ (in Vickers), respectively. As mentioned in section 3.2.1, the values of $HPFL$ and HFZ are 300 and 410 Vickers, respectively. Values of P and f are 1 and 0.5, respectively. Using this equation, D_c is calculated to be 8.8 mm, which is very similar to the experimental results achieved in this research.

4. Conclusion

In this research, the microstructural and mechanical properties of dissimilar DP780/DP980 resistance spot welds are investigated. The most remarkable achieved results are:

- 1) Microstructure of the weld nugget is mainly martensitic.
- 2) At both steels, the heat-affected zone is comprised of three distinct regions, namely upper critical, inter critical, and sub-critical heat affected zones. The difference in heat input and a peak temperature of these regions results in different microstructures, which contain martensite, martensite + ferrite, and tempered martensite + ferrite, for UCHAZ, ICHAZ, and SCHAZ, respectively.
- 3) Microhardness test results showed that the hardness of the fusion zone is ~410 HV. Additionally, softening was observed at the SCHAZ regions.
- 4) Changes in weld nugget diameter with welding current showed that nugget diameter first increases with welding currents up to 11 kA, and then decreases as a result of expulsion.
- 5) Values of peak load and fracture energy of the joints increase with welding currents up to 11 kA and then decrease. At 11 kA, the values of peak load and fracture energy are 80 kN and 30 J, respectively.
- 6) The results showed that changing from IF to PF mode occurred at welding currents of 10 kA. The critical weld nugget diameter was 8.5 mm.

References

- [1] Pouranvari M, Marashi SPH (2013) Critical review of automotive steels spot welding: process, structure and properties. *Sci Technol Weld Join* 18:361–403. <https://doi.org/10.1179/1362171813Y.0000000120>
- [2] Pouranvari M, Marashi SPH (2012) Weld nugget formation and mechanical properties of three-sheet resistance spot welded low carbon steel. *Can Metall Q* 51:105–109. <https://doi.org/10.1179/1879139511Y.0000000028>

- [3] Pouranvari M, Mousavizadeh SM, Marashi SPH, et al (2011) Influence of fusion zone size and failure mode on mechanical performance of dissimilar resistance spot welds of AISI 1008 low carbon steel and DP600 advanced high strength steel. *Mater Des* 32:1390–1398
- [4] Pouranvari M, Marashi SPH (2012) On failure mode of resistance spot welded DP980 advanced high strength steel. *Can Metall Q* 51:447–455. <https://doi.org/10.1179/1879139512Y.0000000034>
- [5] Gould JE, Khurana SP, Li T (2006) Predictions of microstructures when welding automotive advanced high-strength steels. *Weld J (Miami, Fla)* 85:
- [6] Hernandez BVH, Kuntz ML, Khan MI, Zhou Y (2008) Influence of microstructure and weld size on the mechanical behaviour of dissimilar AHSS resistance spot welds. *Sci Technol Weld Join* 13:769–776. <https://doi.org/10.1179/136217108X325470>
- [7] Ghaemifar S, Mirzadeh H (2017) Enhanced mechanical properties of dual-phase steel by repetitive intercritical annealing. *Can Metall Q* 56:459–463. <https://doi.org/10.1080/00084433.2017.1361223>
- [8] Shukla N, Roy H, Show BK (2016) Effect of prior austempering heat treatment on the microstructure, mechanical properties and high-stress abrasive wear behaviour of a 0.33% C dual-phase steel. *Can Metall Q* 55:13–22. <https://doi.org/10.1080/00084433.2015.1113671>
- [9] Zhang H, Qiu X, Bai Y, et al (2014) Resistance spot welding macro characteristics of the dissimilar thickness dual phase steels. *Mater Des* 63:151–158. <https://doi.org/10.1016/J.MATDES.2014.05.060>
- [10] Abadi MMH, Pouranvari M (2014) Failure-mode transition in resistance spot welded DP780 advanced high-strength steel: Effect of loading conditions. *Mater Tehnol* 48:67–71
- [11] Khan MI, Kuntz ML, Zhou Y (2008) Effects of weld microstructure on static and impact performance of resistance spot welded joints in advanced high strength steels. *Sci Technol Weld Join* 13:294–304. <https://doi.org/10.1179/174329308X271733>
- [12] Pouranvari M (2011) Influence of welding parameters on peak load and energy absorption of dissimilar resistance spot welds of DP600 and AISI 1008 steels. *Can Metall Q* 50:381–388. <https://doi.org/10.1179/1879139511Y.0000000008>
- [13] Zhang H, Wei A, Qiu X, Chen J (2014) Microstructure and mechanical properties of resistance spot welded dissimilar thickness DP780/DP600 dual-phase steel joints. *Mater Des* 54:443–449.

<https://doi.org/10.1016/J.MATDES.2013.08.027>

[14] Liang J, Zhang H, Qiu X, Shi Y (2015) Characteristics of the Resistance Spot Welding Joints in Dissimilar Thickness Dual-phase Steels. *ISIJ Int* 55:2002–2007.

<https://doi.org/10.2355/isijinternational.ISIJINT-2015-151>

[15] Di H, Sun Q, Wang X, et al (2017) Microstructure and properties in dissimilar/similar weld joints between DP780 and DP980 steels processed by fiber laser welding. *J Mater Sci Technol* 33:1561–1571.

<https://doi.org/10.1016/j.jmst.2017.09.001>

[16] Pouranvari M, Marashi SPH, Mousavizadeh SM (2010) Failure mode transition and mechanical properties of similar and dissimilar resistance spot welds of DP600 and low carbon steels. *Sci Technol Weld Join* 15:625–631.

<https://doi.org/10.1179/136217110X12813393169534>

[17] Gao S, Li Y, Yang L, Qiu W (2018) Microstructure and mechanical properties of laser-welded dissimilar DP780 and DP980 high-strength steel joints. *Mater Sci Eng A* 720:117–129. <https://doi.org/10.1016/J.MSEA.2018.02.057>

[18] Wei ST, Lv D, Liu RD, et al (2014) Similar and dissimilar resistance spot welding of advanced high strength steels: welding and heat treatment procedures, structure and mechanical properties. *Sci Technol Weld Join* 19:427–435.

<https://doi.org/10.1179/1362171814Y.0000000211>

[19] Pouranvari M, Marashi SPH (2010) Key factors influencing mechanical performance of dual phase steel resistance spot welds. *Sci Technol Weld Join* 15:149–155.

<https://doi.org/10.1179/136217109X12590746472535>

[20] Liu C, Zheng X, He H, et al (2016) Effect of

work hardening on mechanical behavior of resistance spot welding joint during tension shear test. *Mater Des* 100:188–197.

<https://doi.org/10.1016/J.MATDES.2016.03.120>

[21] Zhang H, Senkara J (2012) Resistance welding: fundamentals and applications. CRC Press, Boca Raton

[22] Wei ST, Liu RD, Lv D, et al (2016) Effect of joint configuration on resistance spot weldability of galvanised DP780 steel sheets. *Sci Technol Weld Join* 21:178–185.

<https://doi.org/10.1179/1362171815Y.0000000081>

[23] Pouranvari M, Marashi SPH (2011) Failure mode transition in AHSS resistance spot welds. Part I. Controlling factors. *Mater Sci Eng A* 528:8337–8343. <https://doi.org/10.1016/J.MSEA.2011.08.017>

[24] American Welding Society. Joint Committee on Automotive Welding., American Welding Society. Technical Activities Committee., American National Standards Institute. Test methods for evaluating the resistance spot welding behavior of automotive sheet steel materials

[25] (2017) JIS Z 3144: Routine test of resistance spot and projection welds, 13th ed. Japanese Standards Association (JSA)

[26] Y. J. Chao (2003) Failure mode of spot welds: interfacial versus pullout. *Sci Technol Weld Join* 8:133–137

[27] Sun X, Stephens E, Khaleel M (2006) Effects of Fusion Zone Size on Failure Modes and Performance of Advanced High Strength Steel Spot Welds. *SAE Trans.* 115:509–516

[28] Pouranvari M, Marashi SPH, Safanama DS (2011) Failure mode transition in AHSS resistance spot welds. Part II: Experimental investigation and model validation. *Mater Sci Eng A* 528:8344–8352. <https://doi.org/10.1016/J.MSEA.2011.08.016>